Electronic Supplementary Material (ESI) for Journal of Materials Chemistry A.

Supporting Information for Manuscript Entitled with

Synthesis of Conductive Microcapsules for Fabricating Restorable Circuits

Yun-Ju Lan,[a] Shinn-Jen Chang[b] and Chia-Chen Li*[a]

[a] Institute of Materials Science and Engineering, and Department of Materials & Mineral Resources Engineering, National Taipei University of Technology, Taipei 10608, Taiwan

[b] Material and Chemical Research Laboratories, Industrial Technology Research Institute, Hsinchu 30011, Taiwan

* Correspondence author. E-mail: ccli@ntut.edu.tw

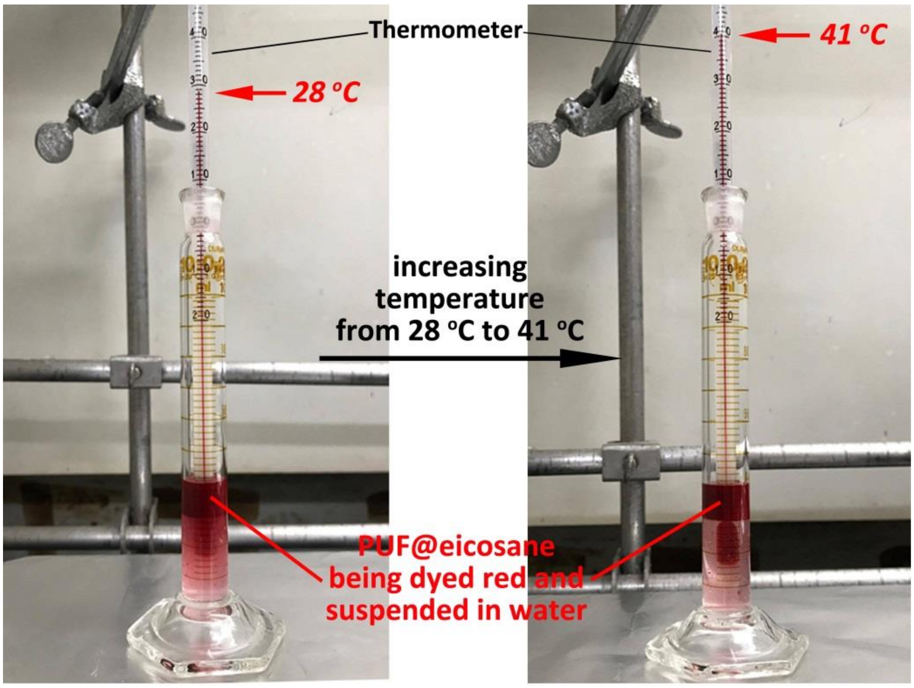

Fig. S1 Photos showing a suspension of PUF@eicosane in water with being warmed by a slowly increased temperature from 28 ^{o}C (room temp.) to 41 ^{o}C (eicosane has melted) at a heating rate of ~ 1 ^{o}C/min.

Fig. S1 shows a simple equipment for testing the volume change of PUF@eicosane under temperature variation. For easier identification, PUF@eicosane was dyed red (Disperse Red-1; 95%, Sigma-Aldrich, USA) and had a high solid loading of 20 vol% in water. The bottom layer of water showed slightly red, which could be due to the very few amount of suspending microcapsules (because the red dye is not water-dissolvable). Clearly, PUF@eicosane showed almost unchanged volume with increasing temperature, corresponding well to the reported property of PCMs in literature.[25]

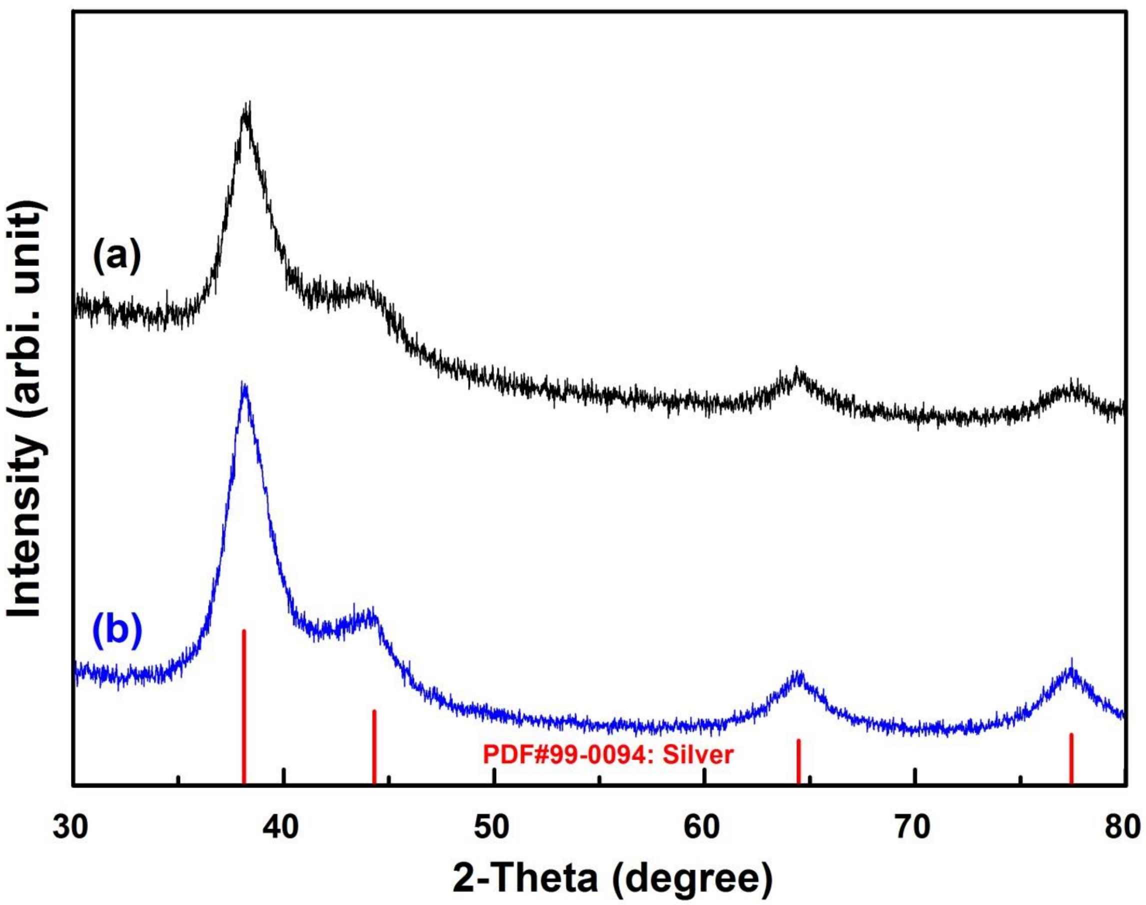

Fig. S2 XRD spectra of the as-synthesized Ag nanopowder: (a) fleshly synthesized; (b) being stored under ambient condition for 3 months.

The fleshly synthesized nano Ag (Fig. S2a) and the nano Ag that has been stored for 3 months (Fig. S2b) show a similar diffraction profile with 2θ peaks at 38.2°, 44.3°, 64.5°, and 77.4°, corresponding to the (111), (200), (220), and (311) crystallographic planes, respectively, of the face-centered cubic (FCC) Ag crystal. Evidently, the synthesized nano Ag has a good chemical stability and is not easily oxidized in spite of being stored under ambient condition for 3 months.

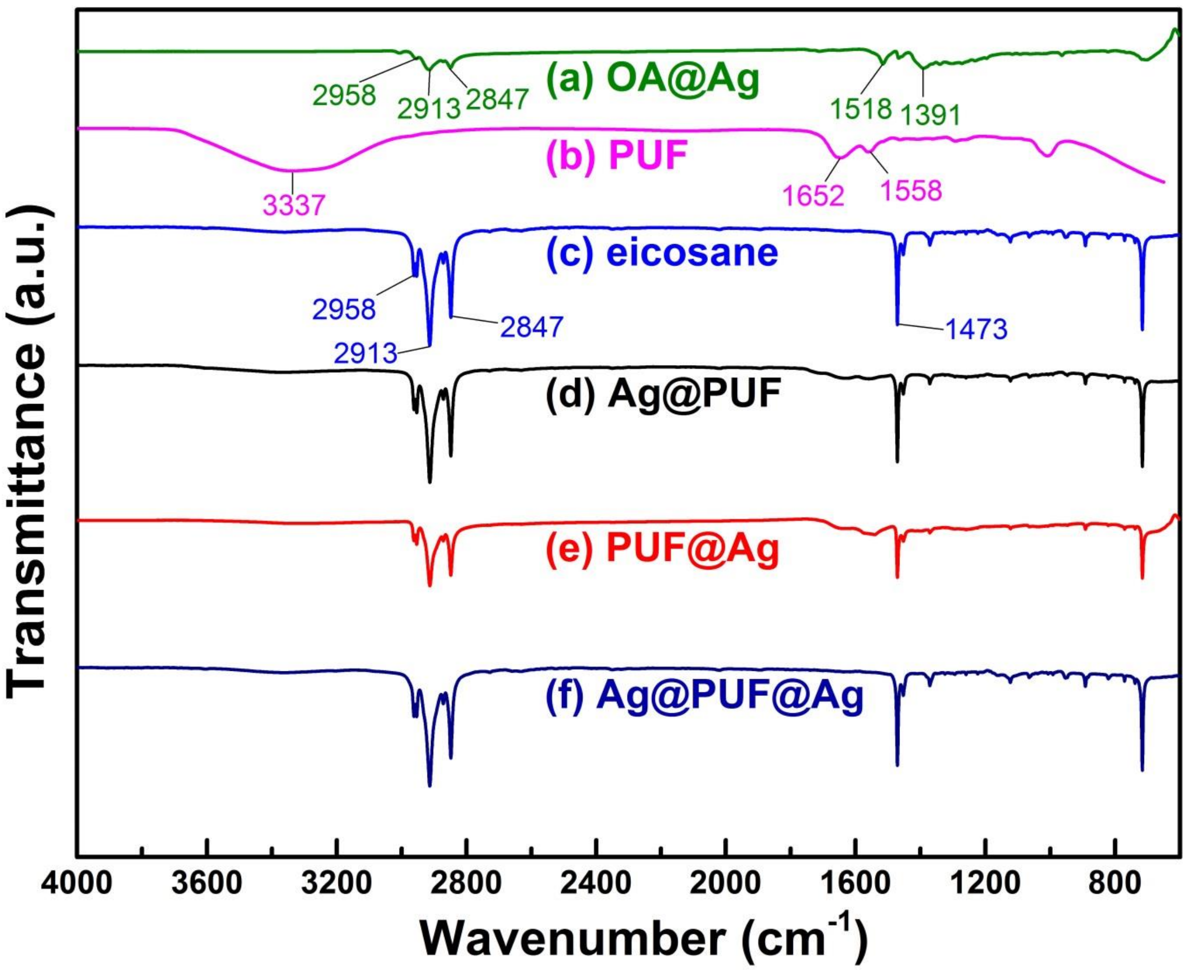

Fig. S3 FT-IR spectra of (a) OA-modified nano Ag particle (OA@Ag), (b) pure PUF, (c) pure eicosane, (d) Ag@PUF, (e) PUF@Ag, and (f) Ag@PUF@Ag.

In Fig. S3a, the IR spectrum shows the characteristic peaks of OA-modified nano Ag (OA@Ag). The absorptions at 2800-3000 cm^{-1} correspond to the C-H stretchings of the alkyl chain present in OA, indicating the presence of OA on nano Ag. In Fig. S3b, the broad band that appears at 3337 cm^{-1} is the IR absorption for the –OH vibration and the peak at 1652 cm^{-1} is attributed to the vibration of the carbonyl group in PUF. In Fig. S3c, eicosane also shows the absorptions at 2800-3000 cm^{-1}, corresponding to the C-H stretchings of the alkyl chain of eicosane; the peak at 1473 cm^{-1} is attributed to the C-H stretching of methylene bridge. In Fig. S3d-f, all the three types of microcapsules show a significant presence of the characteristic absorptions belonging to PUF and eicosane, indicating the eicosane has been successfully encapsulated by PUF. However, the characteristic absorptions of OA@Ag (Fig. S3a) are too weak and overlap with eicosane (Fig. S3c) at 2800-3000 cm^{-1} and 1400-1500 cm^{-1}, and therefore, the absorptions attributed to OA@Ag are difficult to be contradistinguished in the results of Fig. S3d-f.

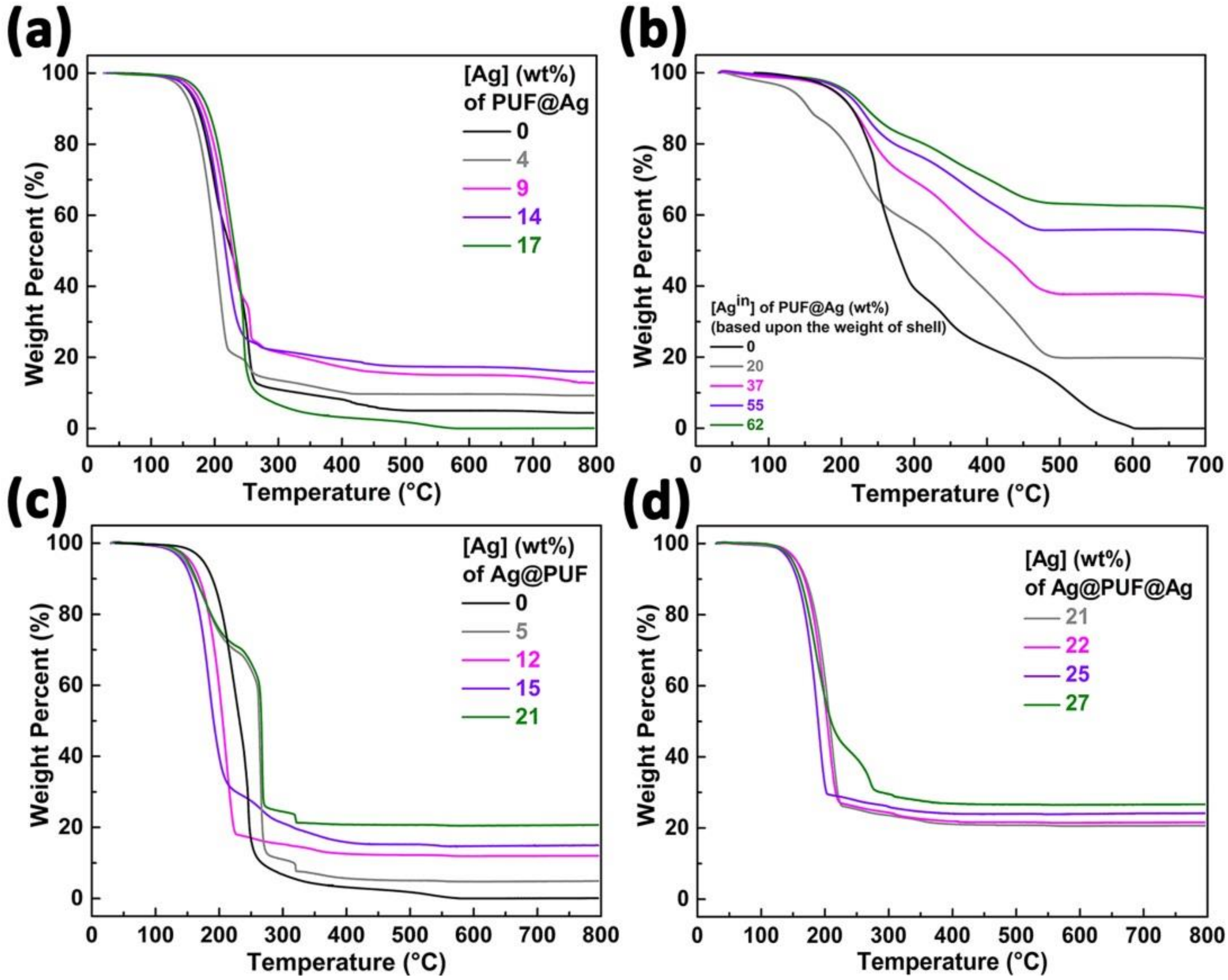

Fig. S4 Thermal gravitational (TG) curves showing the weight loss of (a) PUF@Ag, (b) shell of PUF@Ag, (c) Ag@PUF, and (d) Ag@PUF@Ag with various [Ag]. The heating rate was 10 °C min^{-1}.

To know the relative distribution concentrations of Ag in the core and at the inner part of the PUF@Ag shell based on the weight of a whole microcapsule, i.e., $[Ag_{scapsule}^{in}]$ and $[Ag_{capsule}^{core}]$, respectively, calculations based upon the TG data in above were conducted in the following.

The weight ratios of Ag shown in Fig. S4a,c,d and Fig. S4b were obtained based on the weights of a whole microcapsule ($[Ag_{capsule}]$) and only shell ($[Ag_{shell}]$ or $[Ag_{shell}^{in}]$), described by Eqs. (S1) and (S2), respectively. For the measurment of Fig. S4b, the core material in the microcapsule has to be removed in advance (see “Experimental“ on page 2 of the main article).

$$\left[Ag_{capsule}\right] = \frac{W_{Ag}^{in}+W_{Ag}^{core}}{W_{shell}+W_{Ag}^{in}+W_{Ag}^{core}+W_{eicosane}} \tag{S1}$$

$$\left[Ag_{shell}\right] = \left[Ag_{shell}^{in}\right] = \frac{W_{Ag}^{in}}{W_{shell}+W_{Ag}^{in}} = x \tag{S2}$$

where W_{Ag}^{in}, W_{Ag}^{core}, W_{shell}, and $W_{eicosane}$ are the weights of Ag at innert part of shell, Ag in the core, PUF shell, and eicosane core, respectively. In other words, the [Ag] (also $[Ag_{capsule}]$) in Fig. S4a was resulted from the summation of the Ag in the core and at the inner part of shell, and [Ag^{in}] (also $[Ag_{shell}^{in}]$) of Fig. S4b was resulted only from the Ag at the inner part of shell. To know the content of Ag in the core based upon the wieght of a whole microcapsule, i.e., $[Ag_{capsule}^{core}]$, the value of $[Ag_{shell}^{in}]$ obtained from Fig. S4b needs to be transferred to $[Ag_{capsule}^{in}]$ that is defined by Eq. (S3), and then to have $[Ag_{capsule}]$ substracted by $[Ag_{capsule}^{in}]$ to obtain $[Ag_{capsule}^{core}]$, as described by Eq. (S4).

$$\left[Ag_{capsule}^{in}\right] = \frac{W_{Ag}^{in}}{W_{shell}+W_{Ag}^{in}+W_{Ag}^{core}+W_{eicosane}} \tag{S3}$$

$$\left[Ag_{capsule}^{core}\right] = \left[Ag_{capsule}\right] - \left[Ag_{capsule}^{in}\right] \tag{S4}$$

According to Eq. (S2), we can have

$$W_{Ag}^{in} = \left(\frac{x}{1-x}\right) W_{shell} \tag{S5}$$

Substituting the W_{Ag}^{in} of Eq. (S3) by Eq. (S5), and then we obtain

$$\left[Ag_{capsule}^{in}\right] = \frac{x\, W_{shell}}{W_{shell}+(1-x)(W_{Ag}^{core}+W_{eicosane})} \tag{S6}$$

In addition, it is known that the weight of a microcapsule (W_t) can be represented by

$$W_t = W_{Ag}^{in} + W_{shell} + W_{Ag}^{core} + W_{eicosane} \tag{S7}$$

and therefore

$$(W_{Ag}^{core} + W_{eicosane}) = Wt - (W_{Ag}^{in} + W_{shell}) = Wt - [\left(\frac{x}{1-x}\right) W_{shell} + W_{shell}] = Wt - (\frac{1}{1-x}) W_{shell} \tag{S8}$$

Substituting the term $(W_{Ag}^{core} + W_{eicosane})$ of Eq. (S6) by Eq. (S8), we can finally obtain

$$\left[Ag_{capsule}^{in}\right] = \frac{x\, W_{shell}}{(1-x)Wt} \tag{S9}$$

where Wt is a known value and x and W_{shell} can be directly obtained from Fig. S4b, and thus $\left[Ag_{capsule}^{in}\right]$ is solved. The content of Ag in the core, i.e., $[Ag_{capsule}^{core}]$, can then be determined by Eq. (S4).

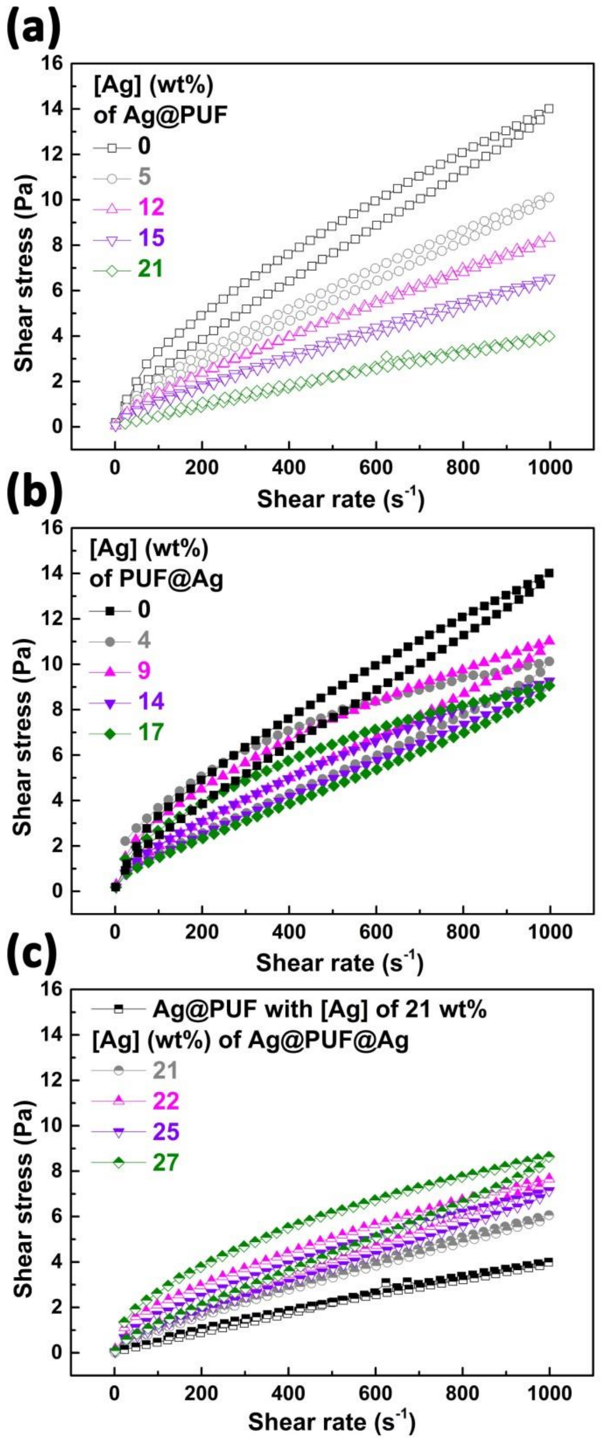

Fig. S5 Shear stress as a function of shear rate for 30 wt% Ag pastes in ethanol containing 20 vol% of (a) Ag@PUF, (b) PUF@Ag, and (c) Ag@PUF@Ag microcapsules with various [Ag].

Fig. S5 compares the rheological hysteresis loops of 30 wt% Ag pastes with 20 vol% additions of different conductive microcapsules with various [Ag]. In Fig. S5a, the paste was originally thixotropic, demonstrating an obvious hysteresis loop between the rate-increasing and rate-decreasing curves. In general, a smaller loop represents a more stable powder dispersion. When the [Ag] of the added Ag@PUF is higher, lower shear stress and smaller hysteresis loop are resulted, indicating that the paste is more a Newtonian behavior. This evidences the improved chemical compatibility of Ag@PUF with the commercial Ag paste while [Ag] is increased. The above result was also observed in the case of PUF@Ag in Fig. S5b; i.e., increased [Ag] resulted in a better compatibility of PUF@Ag with the Ag paste. However, it is interesting to find that neither the shear stress nor the hysteresis loop became smaller with the increase of [Ag] of Ag@PUF@Ag in Fig. S5c. It has been observed that the available amount of Ag^{out} on Ag@PUF@Ag will be limited by the pre-added Ag^{in} in Ag@PUF@Ag (Fig. 5); that is, [Ag^{out}] decreases with the increase of [Ag^{in}]/or [Ag] of Ag@PUF@Ag. As it is believed that the surface property of Ag@PUF@Ag should be more affected by the surface Ag^{out} than by Ag^{in} or Ag^{core}, the increased [Ag], corresponding to decreased [Ag^{out}], is reasonable to result in a poorer compatibility and dispersity of Ag@PUF@Ag in the commercial Ag paste in Fig. S5c.

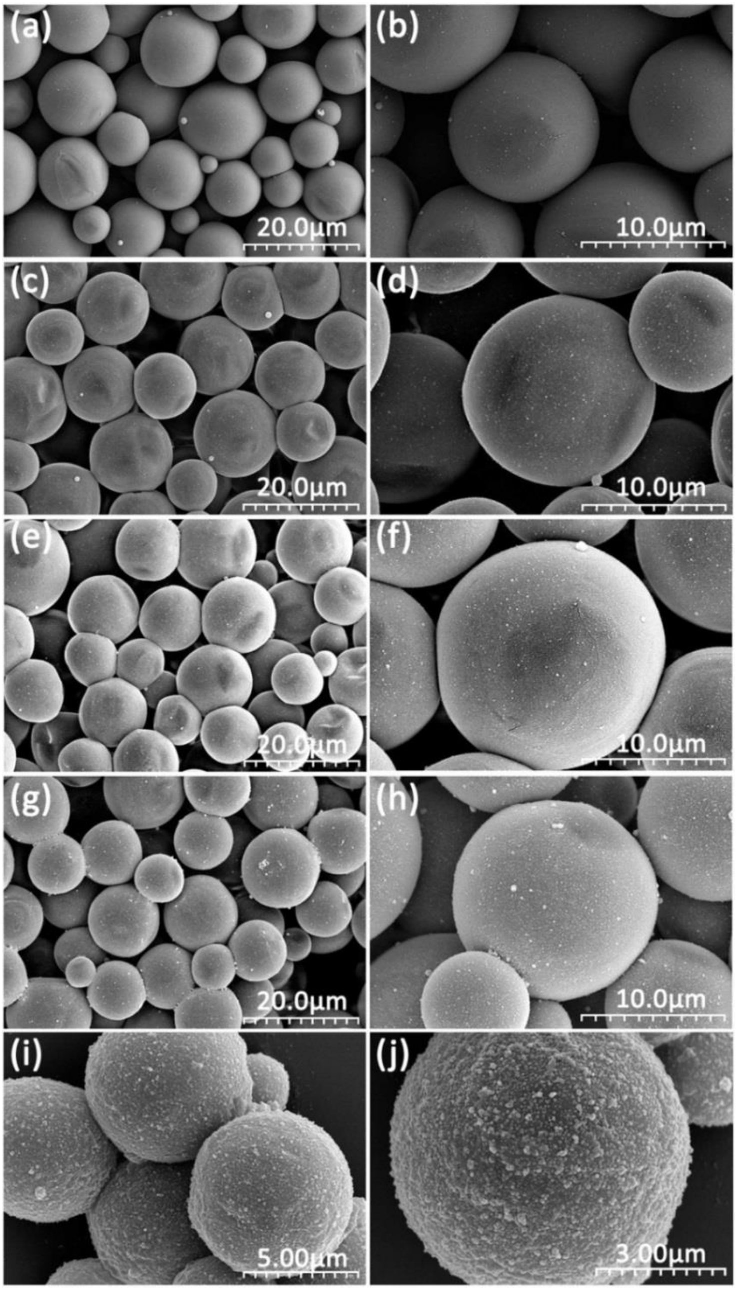

Fig. S6 SEM images of Ag@PUF microcapsules with various [Ag] of (a,b) 0, (c,d) 5, (e,f) 12, (g,h) 15, and (i,j) 21 wt% at different magnifications.

In Fig. S6, it is obvious that the coating of the nano Ag on the microcapsule surface becomes more significant and thicker when the Ag content is increased. Also, the Ag nanoparticles are homogeneously distributed on the microcapsule surface in all the Ag@PUF microcapsules with various [Ag].

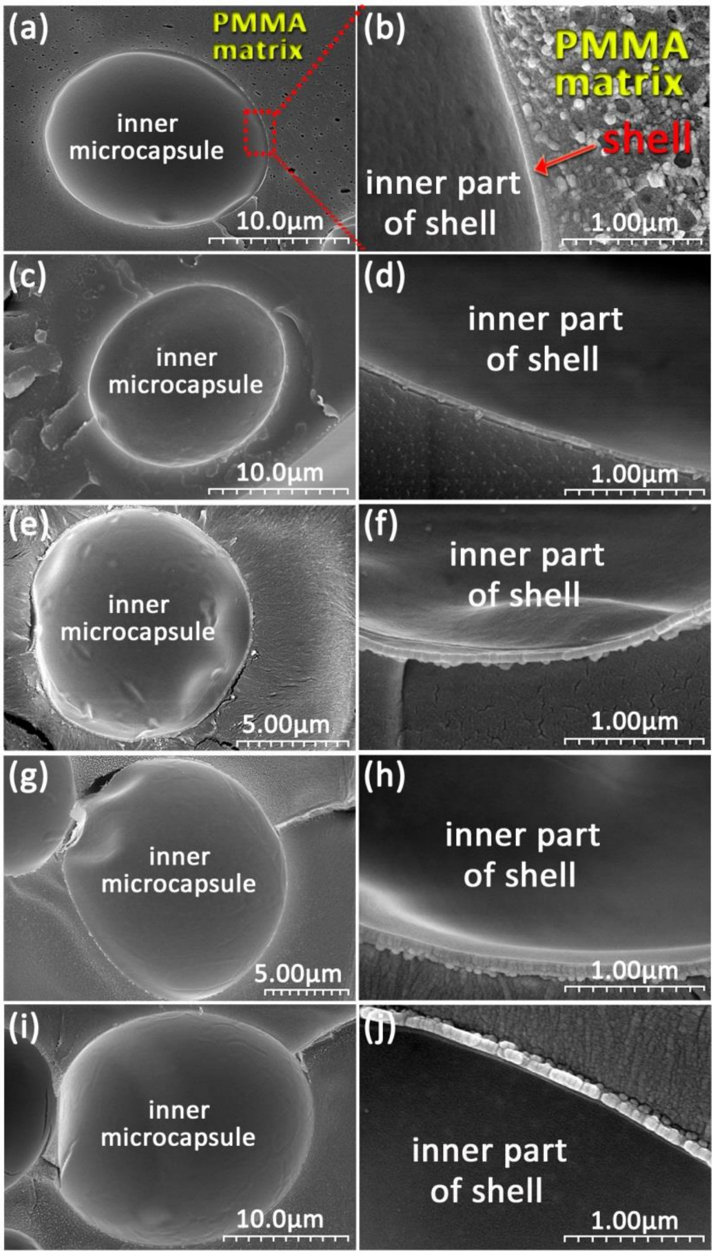

Fig. S7 Cross-sectional (SEM) images of Ag@PUF microcapsules with various [Ag] of (a,b) 0, (c,d) 5, (e,f) 12, (g,h) 15, and (i,j) 21 wt% at different magnifications.

The microcapsules for SEM observations of cross-sectional images were embedded in a poly(methyl methacrylate) (PMMA) matrix and then snapped to break after being immersed in liquid nitrogen for 3 min. The cross-sectional images in Figs. S7a, c, e, g, and i show the absence of nano Ag at the inner part of the Ag@PUF shell. Figs. S7b, d, f, h, and j show the magnified images near the border between the microcapsule and the PAAM matrix.

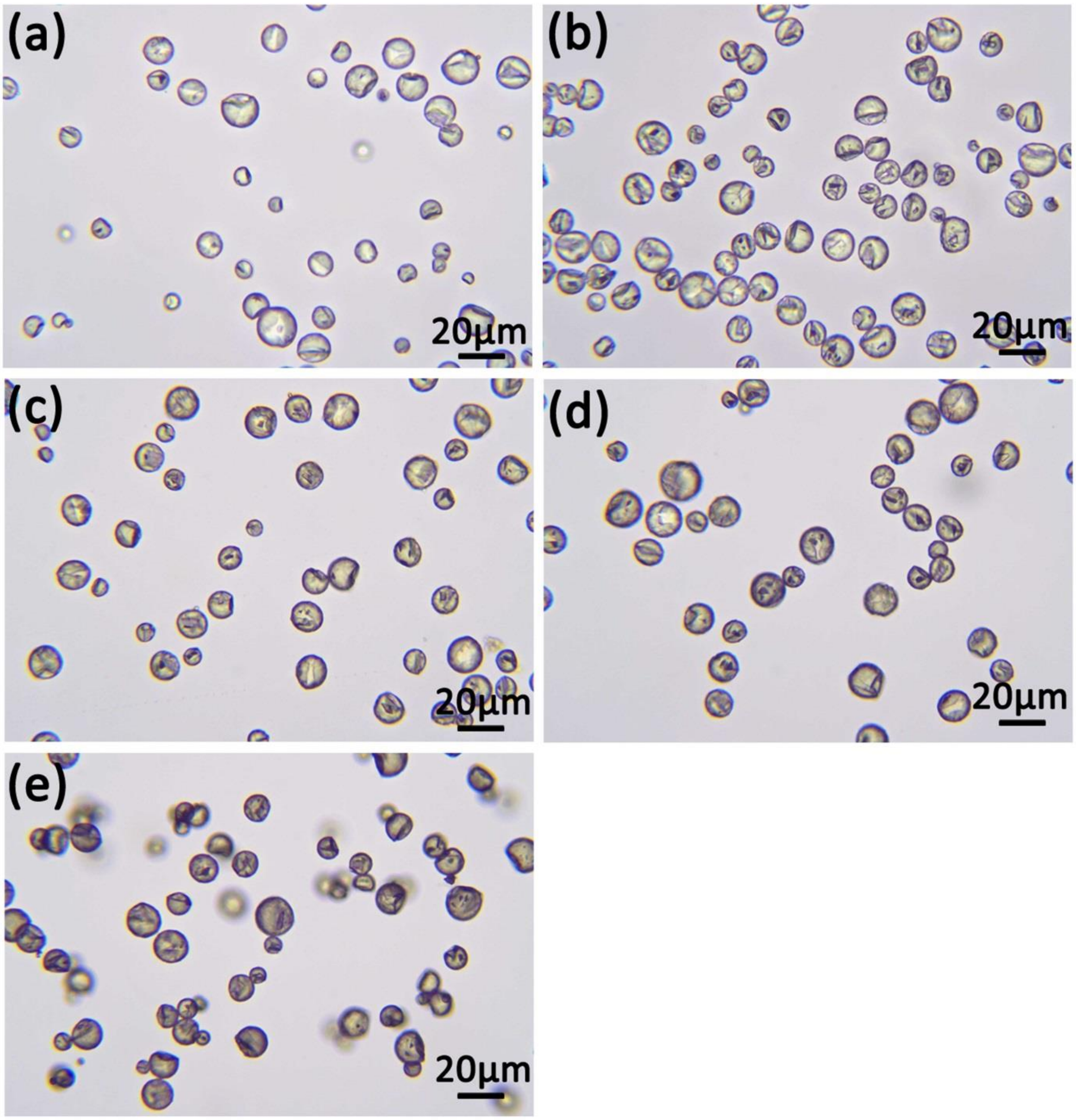

Fig. S8 OM images of Ag@PUF microcapsules with various [Ag] of (a) 0, (b) 5, (c) 12, (d) 15, and (e) 21 wt%.

The transparency of the Ag@PUF microcapsule decreases with the increase of coating amount of nano Ag on the surface, decreasing from Fig. S8a to Fig. S8e. In addition, the uniform distribution of the brown color for each type of microcapsules indicates that the coating of nano Ag is very homogeneous.

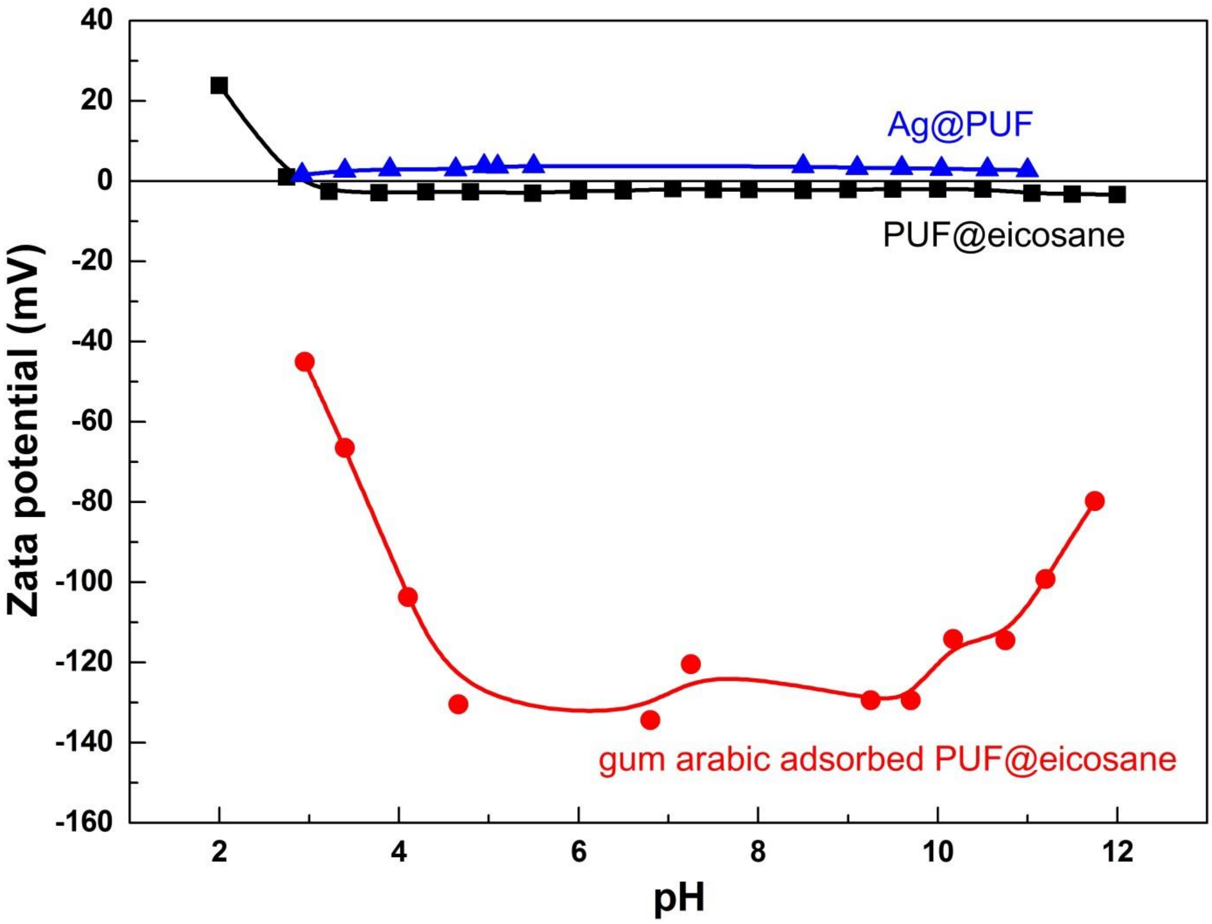

Fig. S9 Zeta potentials of various microcapsules in de-ionized water with a solid loading of 0.5 wt%.

The zeta potentials of PUF@eicosane are mostly within 0 ~ -5 mV (black square). With the addition of 2.5 wt% gum arabic (based upon the weight of PUF@eicosane), the zeta potentials of PUF@Ag significantly shifted to be very negative at ~ -130 mV (red circle). After reduction of Ag on the surface of PUF@eicosane, the zeta potential of the resulting Ag@PUF exhibited zeta potentials within 0 ~ +3 mV, resembling the characteristic surface chemistry of metallic Ag.

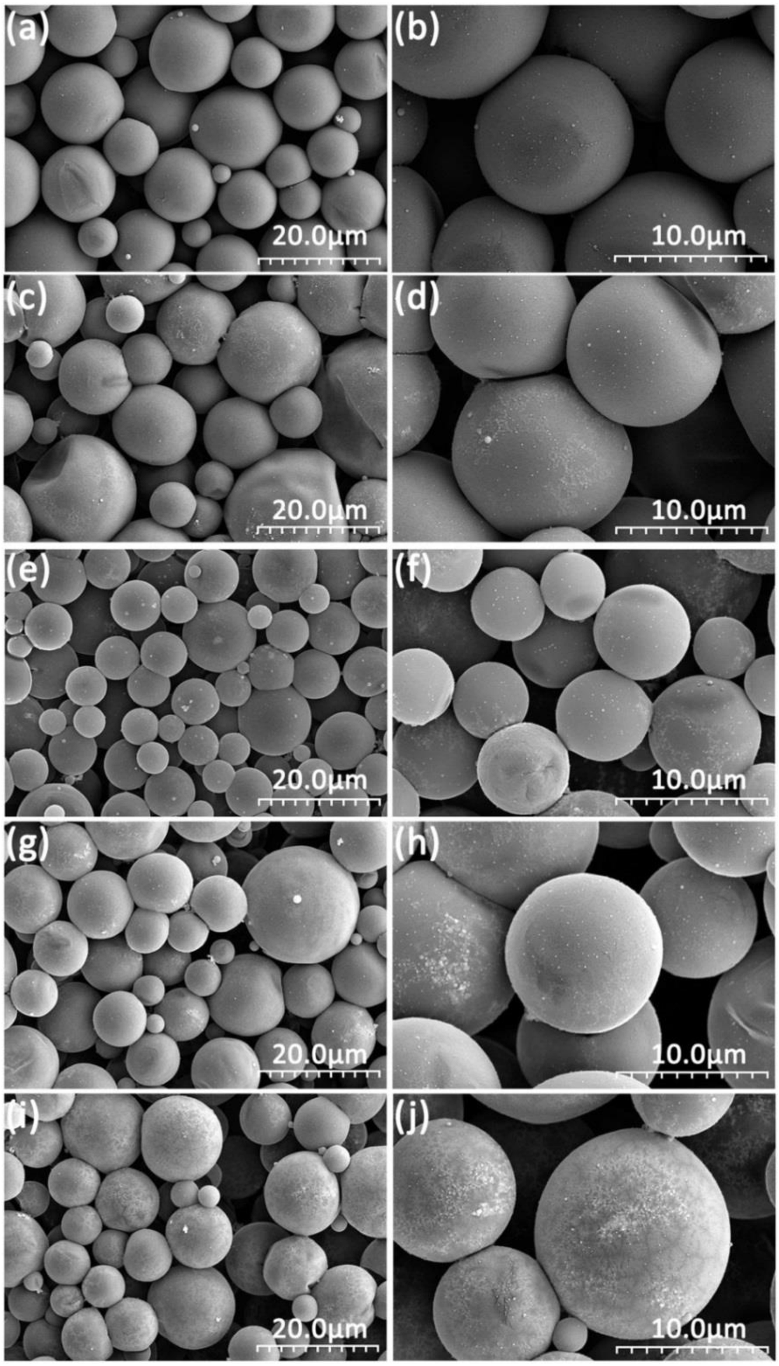

Fig. S10 SEM images of PUF@Ag microcapsules with various [Ag] of (a,b) 0, (c,d) 4, (e,f) 9, (g,h) 14, and (i,j) 17 wt% at different magnifications.

With the increase of [Ag] in the microcapsule, the microcapsule surface appears with more complicated texture, which is suggested to be due to the deeply embedded nano Ag at the inner part of the PUF@Ag shell.

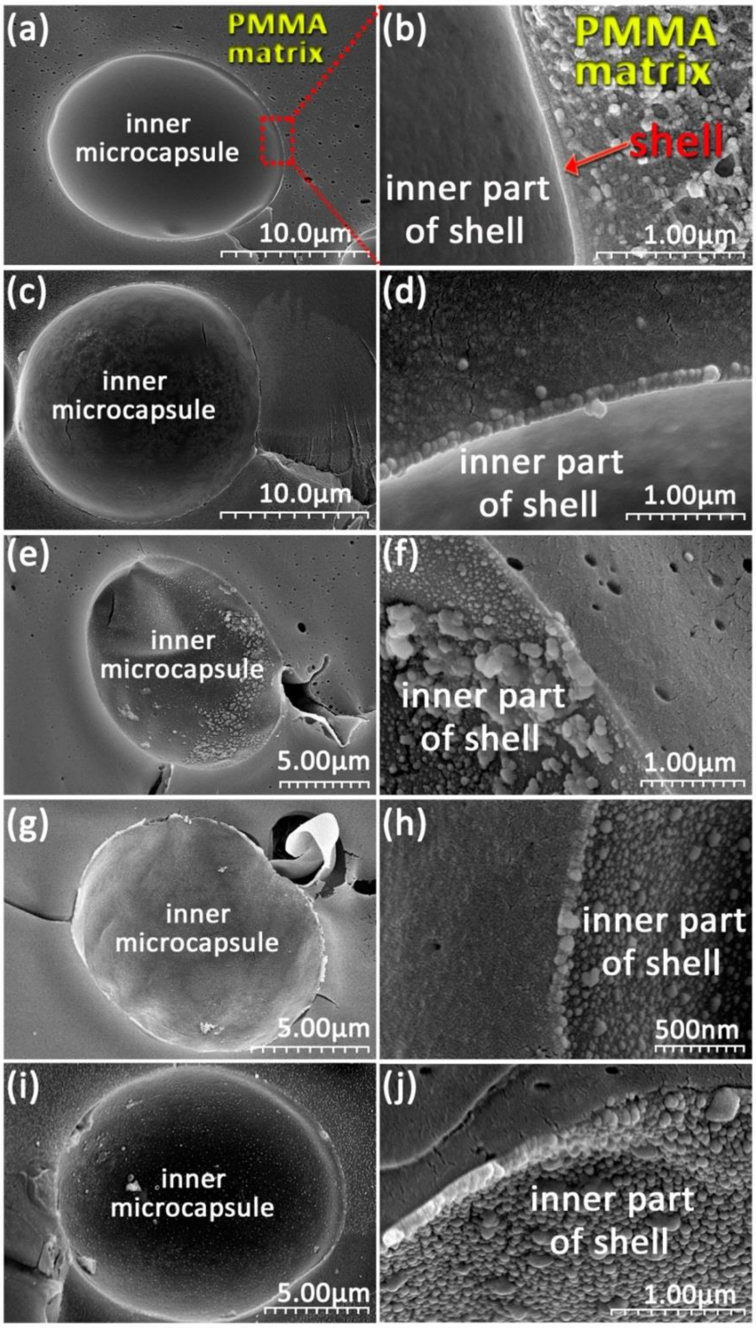

Fig. S11 Cross-sectional (SEM) images of PUF@Ag microcapsules with various [Ag] of (a,b) 0, (c,d) 4, (e,f) 9, (g,h) 14, and (i,j) 17 wt% at different magnifications.

Fig. S11 shows the distribution of the nano Ag embedded at the inner part of PUF@Ag, which higher uniformity is obtained as the [Ag] of the microcapsule is increased, especially when [Ag] is higher than 9 wt%.

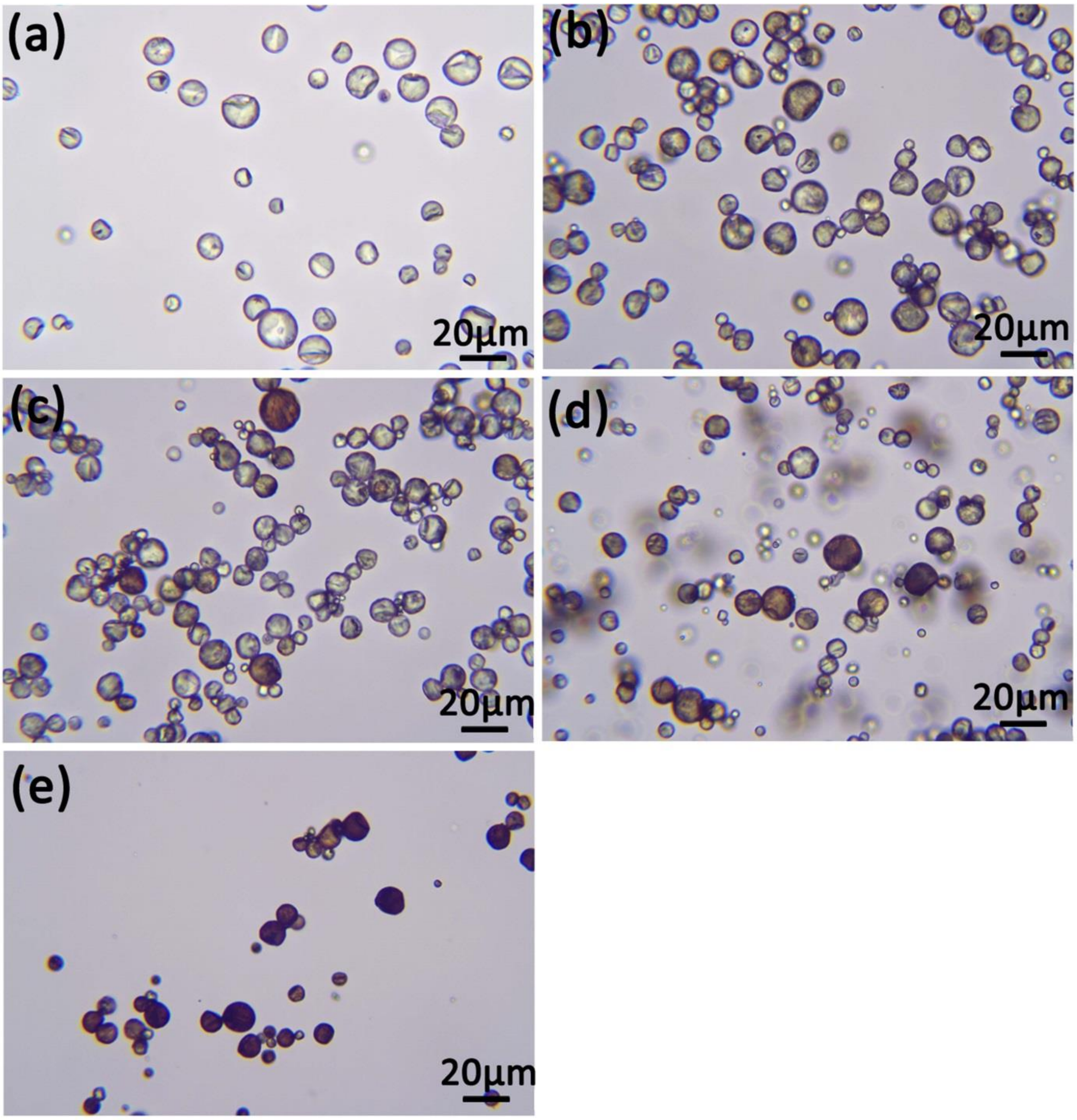

Fig. S12 OM images of PUF@Ag microcapsules with various [Ag] of (a) 0, (b) 4, (c) 9, (d) 14, and (e) 17 wt%.

Fig. S12 shows that the distribution homogeneity of the nano Ag at the inner part of PUF@Ag shell is not as good as that in the case of Ag@PUF, but the detailed reason is still unclear. The color of Ag@PUF is not very uniform until [Ag] is as high as 14-17 wt%.

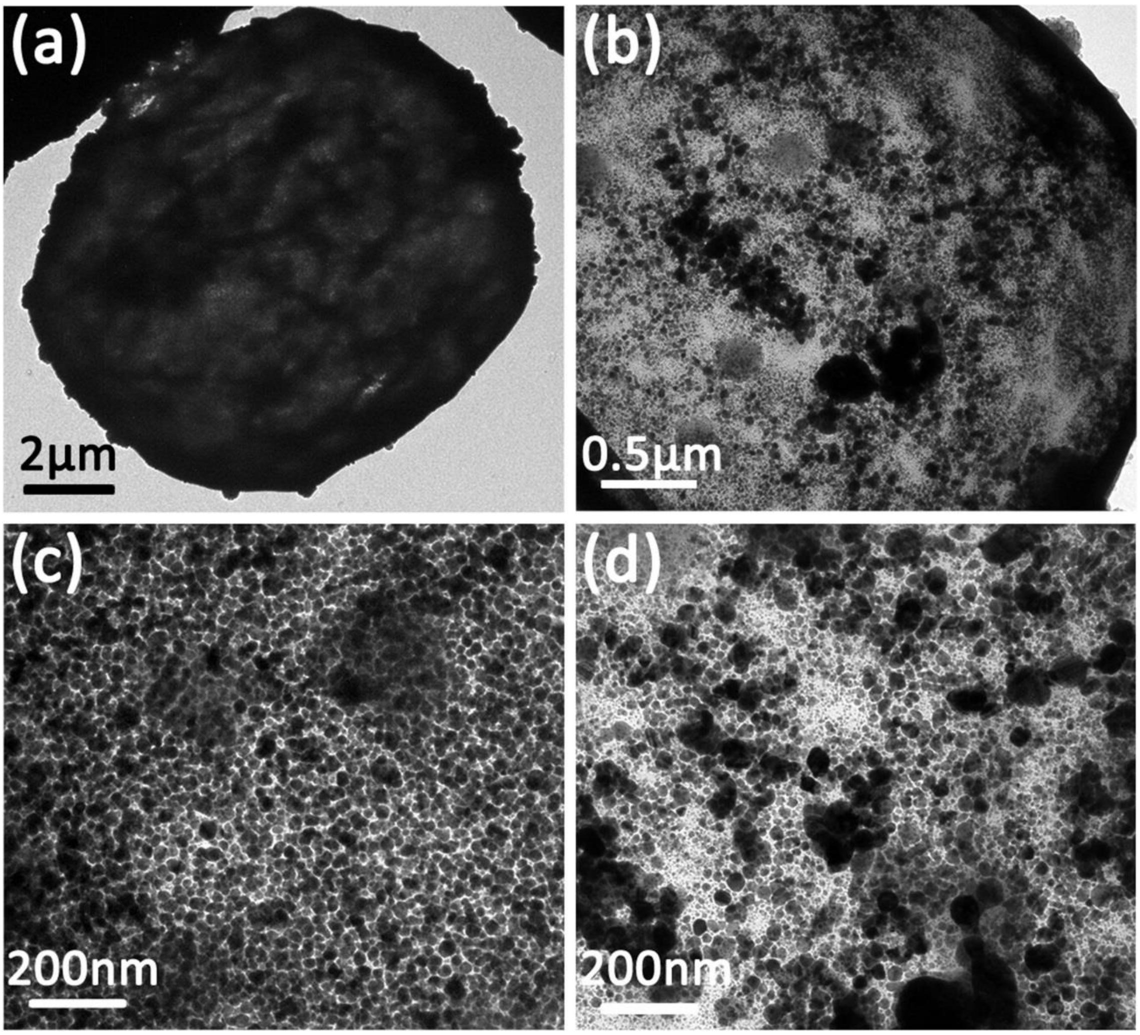

Fig. S13 TEM images of two individual PUF@Ag microcapsules, (a,c) and (b,d), with [Ag] of 17 wt% at different magnifications.

Fig. S13 shows the improved distribution homogeneity of the nano Ag at the inner shell of PUF@Ag at high [Ag] of 17 wt%. The particle growth of nano Ag was observed at some area of the microcapsule, which could be due to the particle agglomeration or Ostwald ripening.[34]

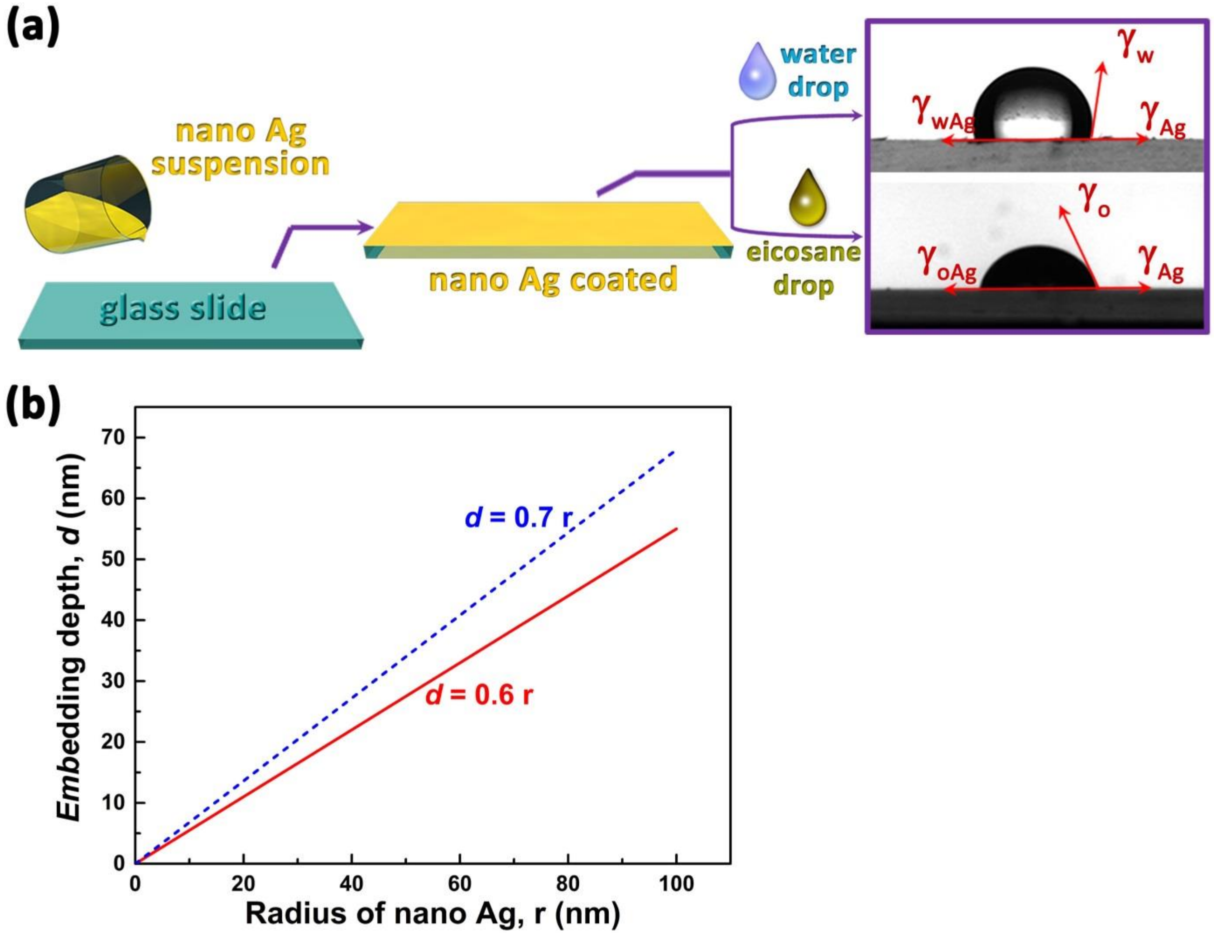

Fig. S14 (a) Experimental procedures for obtaining γ_{wAg} and γ_{oAg}. (b) The embedding depth (*d*) of the nano Ag in the microcapsule shell as a function of the radius (r) of the nano Ag.

To determine the embedding depth (*d*) of the nano Ag in the microcapsule shell by Eq. (2), the value of θ can also be determined by the measurements of surface tensions of water-Ag (γ_{wAg}) and eicosane-Ag (γ_{oAg}). According to Fig. 4c, it is known that Young's equation relating to γ_{wAg}, γ_{oAg}, γ_{ow}, and θ is

$$\gamma_{ow}\cos\theta + \gamma_{wAg} = \gamma_{oAg} \tag{S10}$$

By transposing, we have

$$\cos\theta = \frac{\gamma_{oAg} - \gamma_{wAg}}{\gamma_{ow}} \tag{S11}$$

where γ_{ow} is known as 40.2 mN m^{-1} obtained from the result of Fig. 4d, but γ_{oAg} and γ_{wAg} are unknown. The Young's relations relating to γ_{wAg} and γ_{oAg} are respectively

$$\gamma_{wAg} + \gamma_w \cos\varphi = \gamma_{Ag} \tag{S12}$$

$$\gamma_{oAg} + \gamma_o \cos\lambda = \gamma_{Ag} \tag{S13}$$

Subtracting Eq. (S12) by Eq. (S13), we have

$$\gamma_{wAg} - \gamma_{oAg} = \gamma_o \cos\lambda - \gamma_w \cos\varphi \tag{S14}$$

Substituting Eq. (S14) into Eq. (S11), we can have

$$\cos\theta = \frac{\gamma_o \cos\lambda - \gamma_w \cos\varphi}{\gamma_{ow}} \tag{S15}$$

Since γ_o (25.9 mN m^{-1}), γ_w (67.9 mN m^{-1}), and γ_{ow} (40.2 mN m^{-1}) are all known values, measuring the contact angles of λ and φ, which are 98^o and 70^o obtained from the experiments related to Fig. S14a, can determine the value of θ. The resulted θ from Eq. (S15) is 117^o, approximating to 109^o predicted by the ΔG calculations.

By Eq. (2), the value of *d* will be 0.6r at θ of 117^o. Therefore, the value of *d* should be approximately 0.6r-0.7r, which is 6-7, 9-11, and 15-18 nm as the size of the nano Ag is 20, 30, and 50 nm, respectively; a bigger nano Ag exhibits a larger embedding depth.

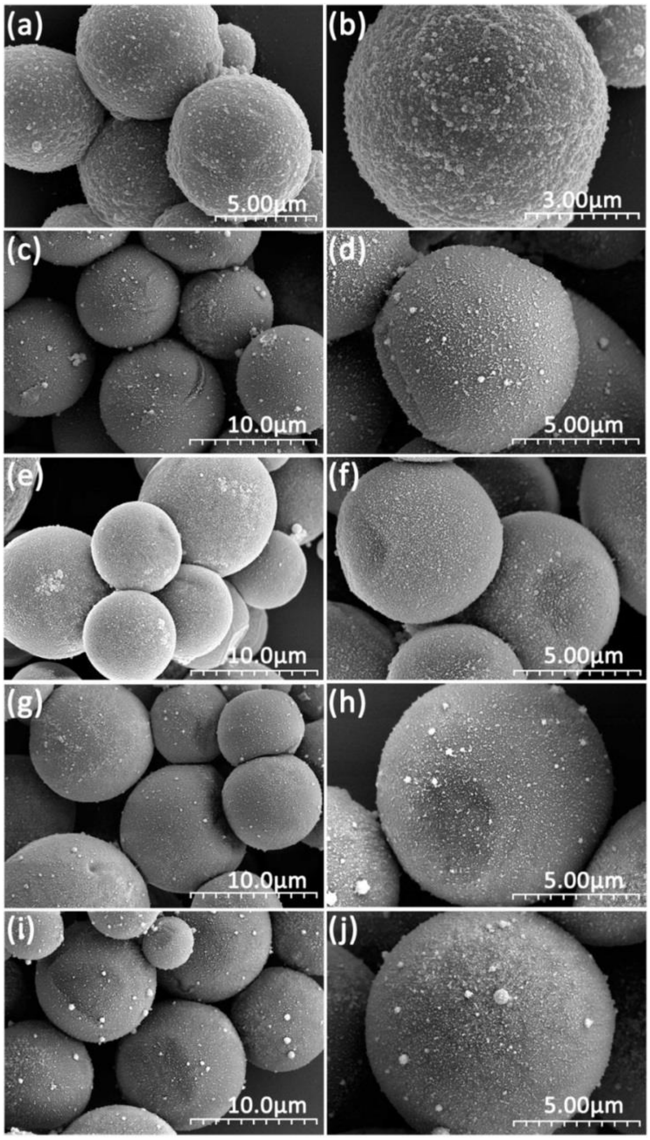

Fig. S15 SEM images of Ag@PUF@Ag microcapsules prepared using the PUF@Ag microcapsules with various [Ag] of (a,b) 0, (c,d) 4, (e,f) 9, (g,h) 14, and (i,j) 17 wt% at different magnifications, corresponding to the Ag@PUF@Ag with [Ag] of (a,b) 21, (c,d) 21, (e,f) 22, (g,h) 25, and (i,j) 27 wt%, respectively.

Fig. S15 shows that the available coating amount of the nano Ag on the outer surface of the Ag@PUF@Ag microcapsule decreased when the nano Ag contained in the core is increased, which more detail has been discussed in “Results and discussion— Properties of Ag@PUF@Ag“ of the main article on page 5-6.

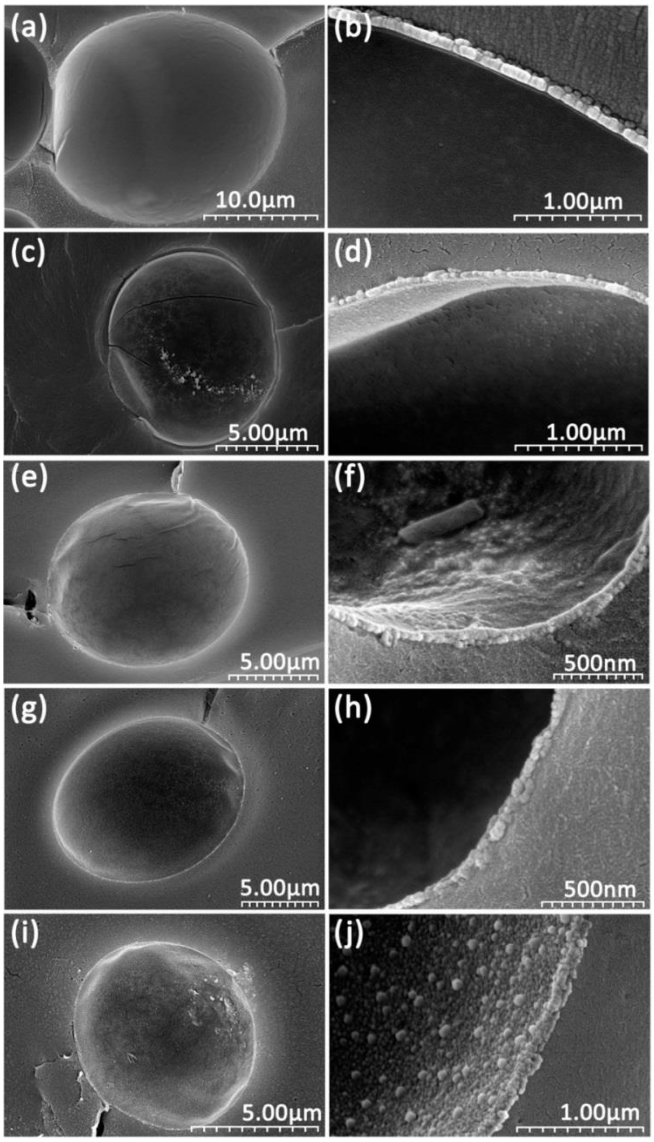

Fig. S16 Cross-sectional (SEM) images of Ag@PUF@Ag microcapsules prepared using the PUF@Ag microcapsules with various [Ag] of (a,b) 0, (c,d) 4, (e,f) 9, (g,h) 14, and (i,j) 17 wt% at different magnifications, corresponding to the Ag@PUF@Ag with [Ag] of (a,b) 21, (c,d) 21, (e,f) 22, (g,h) 25, and (i,j) 27 wt%, respectively.

The result of Fig. S16 just evidences that the increased [Ag] of the Ag@PUF@Ag microcapsule is primarily due to the increased amount of the nano Ag in the core ([Ag^{core}] + [Ag^{in}]), and this is because the amount of Ag^{out} is hardly increased while the Ag content in the core is high, as has shown in Fig. S15 and also mentioned in Fig. 5j of the main article on page 6.

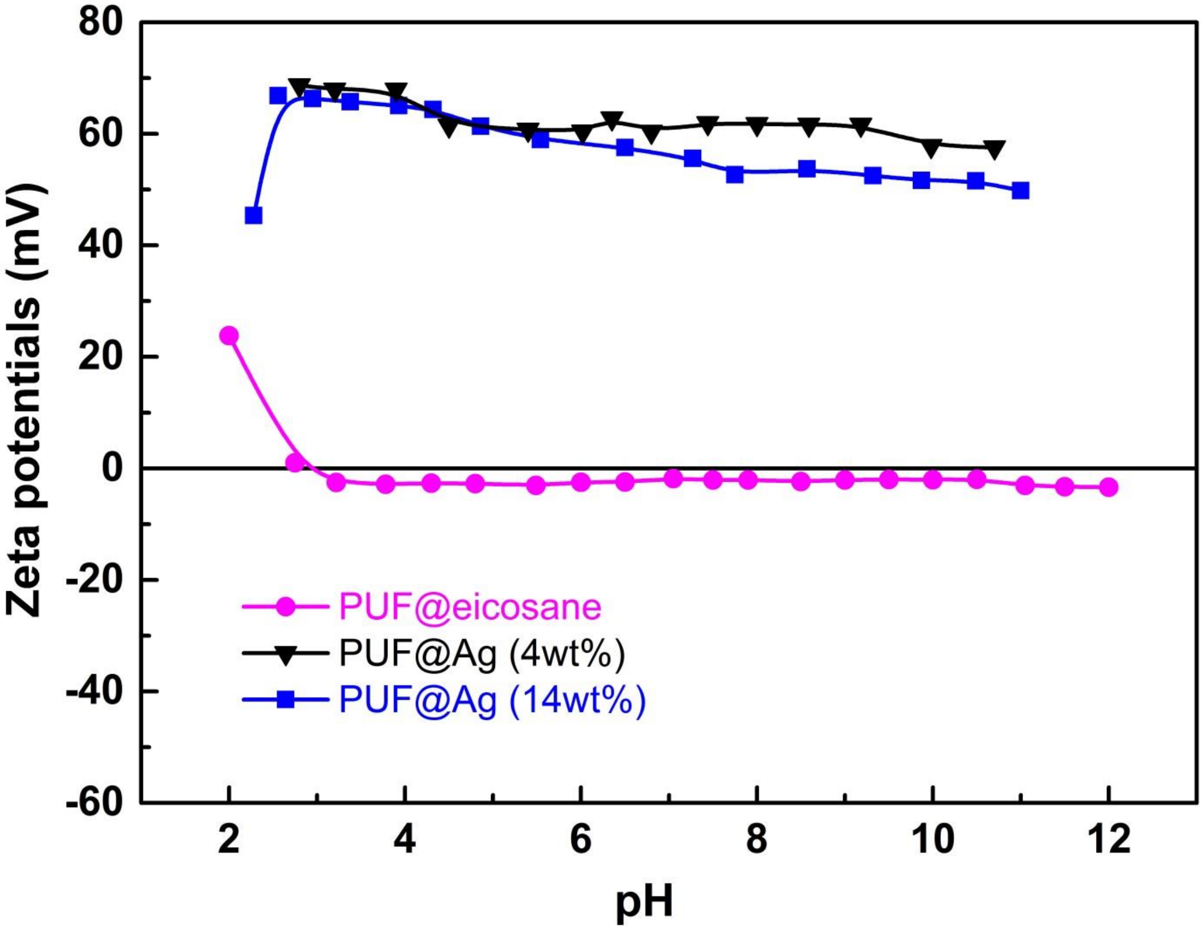

Fig. S17 Zeta potentials of various microcapsules in aqueous suspensions with a solid loading of 0.5 wt%.

The zeta potentials of PUF@eicosane were near 0 mV initially and increased to be very positive at ~ +60 mV when nano Ag was contained. This very positive surface may repel the adsorption of the positively charged $[Ag(NH_3)_2]^+$ and thus reduce the final amount of nano Ag on the microcapsule surface.

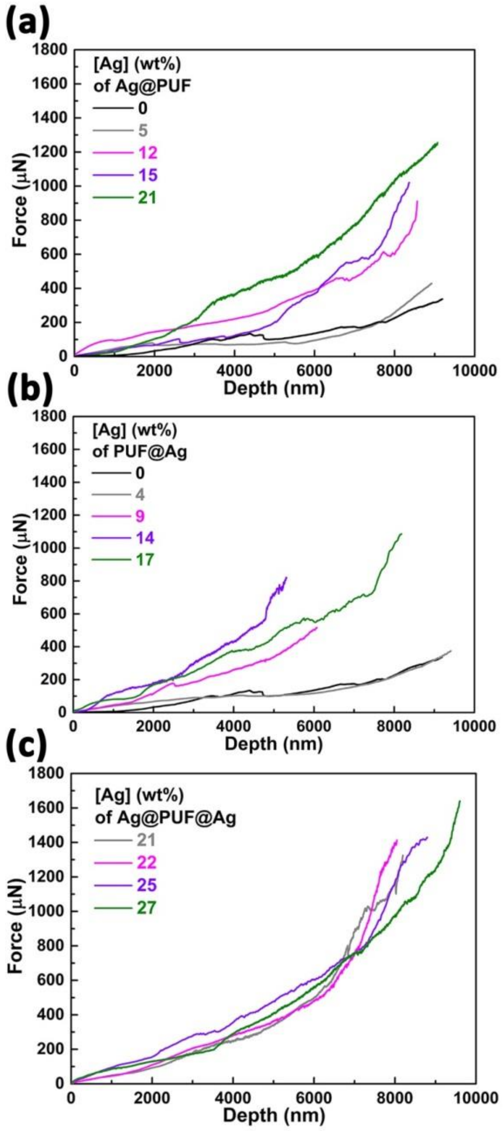

Fig. S18 Loading-displacement curves of (a) Ag@PUF, (b) PUF@Ag, and (c) Ag@PUF@Ag microcapsules with various [Ag].

Fig. S18 shows the loading-displacement curves of various microcapsules with different [Ag]. Typically, elastic materials will show a concave-up curve and the complicated curves shown in Fig. S18 should be attributed to the complex composition of microcapsules, comprising organic and inorganic materials in simultaneous. In addition, the maximum loading force (P_{max}) is generally related to the strength of a material; i.e., mechanically stronger materials show higher values of P_{max}.

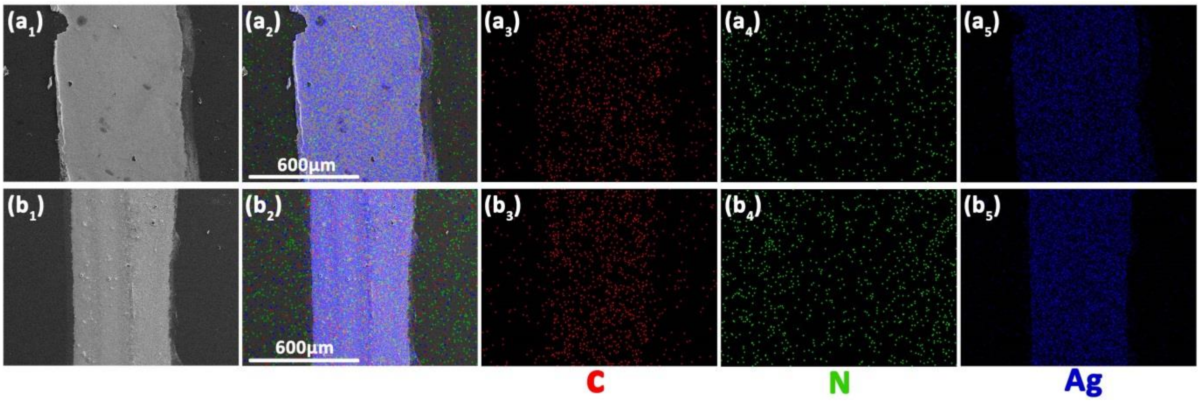

Fig. S19 (a_1,b_1) SEM images and (a_2-a_5,b_2-b_5) EDS elemental mappings of the top views of the Ag circuit lines fabricated by several applications of spray coating of nano Ag ink containing (a_1-a_5) none and (b_1-b_5) 20 vol% of Ag@PUF.

From the comparison on the Ag circuits containing without (a_1-a_5) and with (b_1-b_5) the presence of 20 vol% Ag@PUF in Fig. S19, it was found that the position of the embedded microcapsules is hard to be identified. This should be because the nano Ag of the ink for casting circuits is always surface modified with a significant amount of organic reagents in order to achieve a highly stable dispersion, and therefore the EDS messages from the carbon and nitrogen of the embedded microcapsules are difficult to be distinguished.

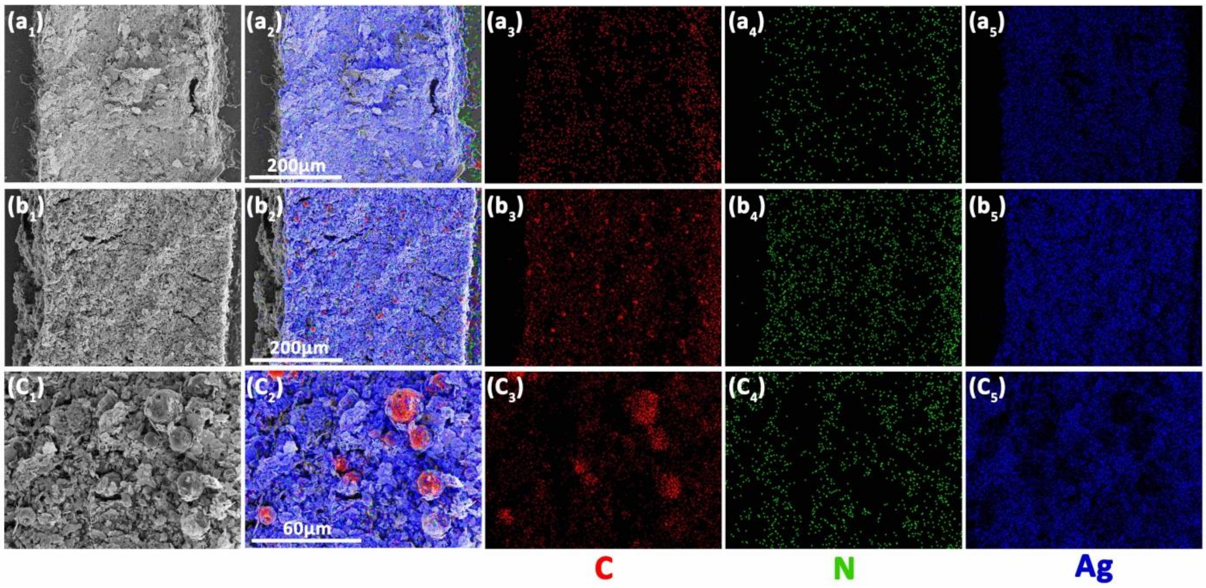

Fig. S20 SEM images (a_1,b_1) and EDS (a_2-a_5,b_2-b_5) elemental mappings of the top views of the Ag circuit lines fabricated by several applications of a spray coating of commercial Ag paste containing (a_1-a_5) none and (b_1-b_5) 20 vol% Ag@PUF. (c_1-c_5) are the magnified images corresponding to (b_1-b_5).

When we replaced the nano Ag ink by the commercial Ag paste for the casting of circuits, the embedded Ag@PUF can then be clearly identified by EDS elemental mapping, as shown in Fig. S20b_1-b_5 and the corresponding magnified images of Fig. S20c_1-c_5. This should be because having excellent stability without showing particle settling is important for the nano Ag ink but is not that a requirement for commercial Ag pastes, and thus most commercial pastes contain much less or even none of organic modifiers, and hence the microcapsules can be contradistinguished from the circuit matrix.

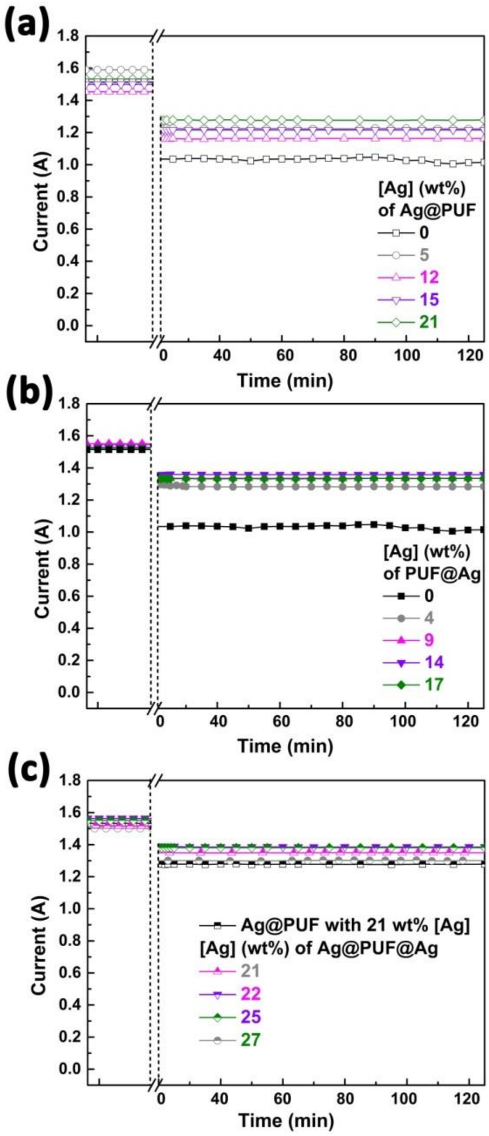

Fig. S21 Variation in electrical current before and after being damaged, including the time period of warming at 38 ^{o}C for 30 sec (the interval between dashed lines, not to scale), for three Ag circuits with and without 20 vol% incorporation of (a) Ag@PUF, (b) PUF@Ag, and (c) Ag@PUF@Ag microcapsules with various [Ag] under a constant applied voltage of 1 V.

Fig. S21 shows the current change of the three types of circuits containing different microcapsules. The current failed to zero instantly while the circuit was interrupted. With 30 sec of warming, the current of various circuits showed a sudden recovery, which efficiency differed from different microcapsule embedment.